

ACCURATE AND SCALABLE ESTIMATION OF EPISTEMIC UNCERTAINTY FOR GRAPH NEURAL NETWORKS

Puja Trivedi*
CSE Department, University of Michigan

Mark Heimann
Lawrence Livermore National Laboratory

Rushil Anirudh
Lawrence Livermore National Laboratory

Danai Koutra
CSE Department, University of Michigan

Jayaraman J. Thiagarajan
Lawrence Livermore National Laboratory

ABSTRACT

Safe deployment of graph neural networks (GNNs) under distribution shift requires models to provide accurate confidence indicators (CI). However, while it is well-known in computer vision that CI quality diminishes under distribution shift, this behavior remains understudied for GNNs. Hence, we begin with a case study on CI calibration under controlled structural and feature distribution shifts and demonstrate that increased expressivity or model size do not always lead to improved CI performance. Consequently, we instead advocate for the use of epistemic uncertainty quantification (UQ) methods to modulate CIs. To this end, we propose G- Δ UQ, a new single model UQ method that extends the recently proposed stochastic centering framework to support structured data and partial stochasticity. Evaluated across covariate, concept, and graph size shifts, G- Δ UQ not only outperforms several popular UQ methods in obtaining calibrated CIs, but also outperforms alternatives when CIs are used for generalization gap prediction or OOD detection. Overall, our work not only introduces a new, flexible GNN UQ method, but also provides novel insights into GNN CIs on safety-critical tasks.

1 INTRODUCTION

As graph neural networks (GNNs) are increasingly deployed in critical applications with test-time distribution shifts (Zhang & Chen, 2018; Gaudelet et al., 2020; Yang et al., 2018; Yan et al., 2019; Zhu et al., 2022), it becomes necessary to expand model evaluation to include safety-centric metrics, such as calibration errors (Guo et al., 2017), out-of-distribution (OOD) rejection rates (Hendrycks & Gimpel, 2017), and generalization gap estimates (Jiang et al., 2019), to holistically understand model performance in such shifted regimes (Hendrycks et al., 2022b; Trivedi et al., 2023b). Notably, such additional metrics often rely on *confidence indicators* (CIs), such as maximum softmax or predictive entropy, which can be derived from prediction probabilities. Although there is a clear understanding in the computer vision literature that the quality of confidence indicators can noticeably deteriorate under distribution shifts (Wiles et al., 2022; Ovidia et al., 2019), and additional factors like model size or expressivity can exacerbate this deterioration (Minderer et al., 2021), the impact of these phenomena on graph neural networks (GNNs) remains under-explored.

Indeed, there is an expectation that adopting more advanced or expressive architectures (Chuang & Jegelka, 2022; Alon & Yahav, 2021; Topping et al., 2022; Rampásek et al., 2022; Zhao et al., 2022) would inherently improve CI calibration on graph classification tasks. Yet, we find that using graph transformers (GTrans) (Rampásek et al., 2022) or positional encodings (Dwivedi et al., 2022a; Wang et al., 2022b; Li et al., 2020) do not significantly improve CI calibration over vanilla message-passing GNNs (MPGNNs) even under controlled, label-preserving distribution shifts. Notably, when CIs are not well-calibrated, GNNs with high accuracy may perform poorly on the additional safety metrics,

*Correspondence to: pujat@umich.edu

leading to unforeseen risks during deployment. Given that using advanced architectures is not an immediately viable solution for improving CI calibration, we instead advocate for modulating CIs using epistemic *uncertainty estimates*.

Uncertainty quantification (UQ) methods (Gal & Ghahramani, 2016; Lakshminarayanan et al., 2017; Blundell et al., 2015) have been extensively studied for vision models (Guo et al., 2017; Minderer et al., 2021), and have been used to improve vision model CI performance under distribution shifts. Our work not only studies the effectiveness of such methods on improving GNN CIs, but also proposes a novel UQ method, G- Δ UQ, which extends the recently proposed, state-of-the-art stochastic data-centering (or ‘‘anchoring’’) framework (Thiagarajan et al., 2022; Netanyahu et al., 2023) to support partial stochasticity and structured data. In brief, stochastic centering provides a scalable alternative to highly effective, but prohibitively expensive, deep ensembles by efficiently sampling a model’s hypothesis space, in lieu of training multiple, independently trained models. When using the uncertainty-modulated confidence estimates from G- Δ UQ, we outperform other popular UQ methods, on not only improving the CI calibration under covariate, concept and graph size shifts, but also in improving generalization gap prediction and OOD detection performance.

Proposed Work. This work studies the effectiveness of GNN CIs on the graph classification tasks with distribution shifts, and proposes a novel uncertainty-based method for improving CI performance. Our contributions can be summarized as follows:

Sec. 2: Case Study on CI Calibration. We find that improving GNN expressivity does not mitigate CI quality degradation under distribution shifts.

Sec. 4: (Partially) Stochastic Anchoring for GNNs. We propose G- Δ UQ, a novel UQ method based on stochastic centering for GNNs with support for partial stochasticity.

Sec. 5: Evaluating Uncertainty-Modulated CIs under Distribution Shifts. Across covariate, concept and graph-size shifts and a suite of evaluation protocols (calibration, OOD rejection, generalization gap prediction), we demonstrate the effectiveness of G- Δ UQ.

2 CASE STUDY ON GNN CI CALIBRATION

In this section, we demonstrate that GNNs struggle to provide calibrated confidence estimates under distribution shift (Dwivedi et al., 2020) despite, improvements in architectures (He et al., 2022; Corso et al., 2020; Zhao et al., 2022) and expressivity (Wang et al., 2022b; Dwivedi et al., 2022a). Since assessing calibration performance does not require any additional, potentially confounding, post-processing, we perform a direct assessment of GNN CI reliability and motivate why uncertainty-based CI modulation is needed.

Notations. Let $\mathcal{G} = (\mathbf{X}, \mathbb{E}, \mathbf{A}, Y)$ be a graph with node features $\mathbf{X} \in \mathbb{R}^{N \times d_\ell}$, (optional) edge features $\mathbb{E} \in \mathbb{R}^{m \times d_\ell}$, adjacency matrix $\mathbf{A} \in \mathbb{R}^{N \times N}$, and graph-level label $Y \in \{0, 1\}^c$, where N, m, d_ℓ, c denote the number of nodes, number of edges, feature dimension and number of classes, respectively. We use i to index a particular sample in the dataset, e.g. $\mathcal{G}_i, \mathbf{X}_i$.

Then, we can define a graph neural network consisting of ℓ message passing layers (MPNN), a graph-level readout function (READOUT), and classifier head (MLP) as follows:

$$\mathbf{X}_M^{\ell+1}, \mathbb{E}^{\ell+1} = \text{MPNN}_e^\ell(\mathbf{X}^\ell, \mathbb{E}^\ell, \mathbf{A}), \quad (1)$$

$$\mathbf{G} = \text{READOUT}(\mathbf{X}_M^{\ell+1}), \quad (2)$$

$$\hat{Y} = \text{MLP}(\mathbf{G}), \quad (3)$$

where $\mathbf{X}_M^{\ell+1}, \mathbb{E}^{\ell+1}$ are intermediate node and edge representations, and \mathbf{G} is the graph representation. We focus on a graph classification setting throughout our paper.

Experimental Set-up: Our experimental set-up is as follows. All results are reported over three seeds.

Models. While improving the expressivity of GNNs is an active area of research, positional encodings (PEs) and graph-transformer (GTran) architectures (Müller et al., 2023) have proven to be particularly popular due to their effectiveness, and flexibility. Indeed, GTrans are known to not only help mitigate over-smoothing (a phenomenon where GNNs lose discriminative power) and over-squashing (a

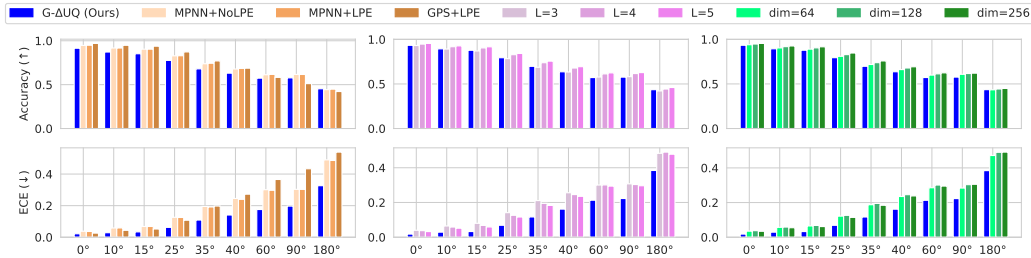


Figure 1: **Calibration on Structural Distortion Distribution Shifts.** On a controlled graph structure distortion shift, we evaluate models trained on the standard superpixel MNIST benchmark (Dwivedi et al., 2020) on super-pixel k -nn graphs created from rotated MNIST images. While accuracy is expected to decrease as distribution shift increases, we observe that the expected calibration error also grows significantly worse. Importantly, this trend is persistent when considering transformer architectural variants (GPS (Rampášek et al., 2022)), as well as different depths and widths. In contrast, our proposed G- Δ UQ method achieves substantial improvement in ECE without significantly compromising on accuracy.

phenomenon where GNNs collapse node representations) (Alon & Yahav, 2021; Topping et al., 2022) but also to better capture long-range dependencies in large graphs (Dwivedi et al., 2022b). Critical to the success of any transformer architecture are well-designed PEs. Notably, graph PEs help improve GNN and GTran expressivity by distinguishing between isomorphic nodes, as well as capturing structural vs. proximity information (Dwivedi et al., 2022a). Here, we ask if these enhancements translate to improved calibration under distribution shift with respect to simple MPNNs by: (i) incorporating equivariant and stable PEs (Wang et al., 2022b); (ii) utilizing MPNN vs. GTran architectures; and, (iii) changing model depth and width. We utilize the state-of-the-art, flexible “general, powerful, scalable” (GPS) GTran (Rampášek et al., 2022) with the GatedGCN backbone. For fair comparison, we use a GatedGCN as the compared MPNN.

Data. Superpixel-MNIST (Dwivedi et al., 2020; Knyazev et al., 2019; Velickovic et al., 2018) is a popular graph classification benchmark that converts MNIST images into k nearest-neighbor graphs of superpixels (Achanta et al., 2012). We select this benchmark as it allows for (i) a diverse set of well-trained models without requiring independent, extensive hyper-parameter search and (ii) controlled, label preserving distribution shifts. Inspired by Ding et al. (2021), we create structurally distorted but valid graphs by rotating MNIST images by a fixed number of degrees and then creating the super-pixel graphs from these rotated images. (See Appendix, Fig. 8.) Since superpixel segmentation on these rotated images will yield different superpixel k -nn graphs without harming class information, we can emulate label-preserving structural distortion shifts. Note, the models are trained only using the original (0° rotation) graphs.

Evaluation. Calibrated models are expected to produce confidence estimates that match the true probabilities of the classes being predicted (Naeini et al., 2015; Guo et al., 2017; Ovadia et al., 2019). While poorly calibrated CIs are over/under confident in their predictions, calibrated CIs are more trustworthy and can also improve performance on other safety-critical tasks which implicitly require reliable prediction probabilities (see Sec. 5). Here, we report the top-1 label expected calibration error (ECE) (Kumar et al., 2019; Detlefsen et al., 2022). Let p_i be the top-1 probability, c_i be the predicted confidence, b_i a uniformly sized bin in $[0, 1]$. Then, $ECE := \sum_i^N b_i ||(p_i - c_i)||$.

Observations. In Fig. 1, we present our results and make the following observations.

Despite the aforementioned benefits in model expressivity, GPS performs noticeably worse compared to the MPGNN, despite having comparable accuracies. This is apparent particularly at severe shifts (60° , 90° , 180° rotations). Furthermore, we find that PEs have minimal effects on both calibration and accuracy. This suggests that while these techniques may enhance theoretical and empirical expressivity, they do not necessarily transfer to the safety-critical task of obtaining calibrated predictions under distribution shifts. In addition, we investigate the impact of model depth and width on calibration performance, considering that model size has been known to affect both the calibration of vision models (Guo et al., 2017; Minderer et al., 2021) and the propensity for over-

squashing in GNNs (Xu et al., 2021). We see that increasing the number of message passing layers ($L = 3 \rightarrow L = 5$) can marginally improve accuracy, but it may also marginally decrease ECE. Moreover, we find that increasing the width of the model can lead to slightly worse calibration at high levels of shift ($90^\circ, 180^\circ$), although accuracy is not compromised.

Notably, when we apply our proposed method G- Δ UQ, (see Sec. 4), to the MPGNN with no positional encodings, it significantly improves the calibration over more expressive variants (GPS, LPE), across all levels of distribution shifts, while maintaining comparable accuracy. We briefly note that we did not tune the hyper-parameters to our method to ensure a fair comparison, so we expect that accuracy could be further improved. Overall, our results emphasize that obtaining reliable GNN CIs remains a difficult problem that cannot be easily solved through advancements in architectures and expressivity. This motivates our uncertainty-modulated CIs as an architecture-agnostic solution.

3 RELATED WORK

Here, we discuss techniques for improving CI reliability and the recently proposed stochastic centering paradigm, before introducing our proposed method in Sec. 4.

3.1 IMPROVING CONFIDENCE INDICATORS

It is well known in computer vision that CIs are often unreliable or uncalibrated directly out-of-the-box (Guo et al., 2017), especially under distribution shifts (Ovadia et al., 2019; Wiles et al., 2022; Hendrycks et al., 2019). Given that reliable CIs are necessary for a variety of safety-critical tasks, including generalization error prediction (GEP) (Jiang et al., 2019) and out-of-distribution (OOD) detection (Hendrycks & Gimpel, 2017), many strategies have been proposed to improve CI calibration (Lakshminarayanan et al., 2017; Guo et al., 2017; Gal & Ghahramani, 2016; Blundell et al., 2015). One particularly effective strategy is to create a deep ensemble (DEns) (Lakshminarayanan et al., 2017) by training a set of independent models (e.g., different hyper-parameters, random-seeds, data order) where the mean predictions over the set is noticeably better calibrated. However, since DEns requires training multiple models, in practice, it can be prohibitively expensive to use. To this end, we focus on single-model strategies.

Single-model UQ techniques attempt to scalably and reliably provide uncertainty estimates, which can then optionally be used to modulate the prediction probabilities. Here, the intuition is that when the epistemic uncertainties are large in a data regime, confidence estimates can be tempered so that they better reflect the accuracy degradation during extrapolation (e.g., training on small-sized graphs but testing on large-sized graphs). Some popular strategies include: Monte Carlo dropout (MCD) (Gal & Ghahramani, 2016) which performs Monte Carlo dropout at inference time and takes the average prediction to improve calibration, temperature scaling (Temp) (Guo et al., 2017) which rescales logits using a temperature parameter computed from a validation set, and SVI (Blundell et al., 2015) which proposes a stochastic variational inference method for estimating uncertainty. While such methods are more scalable than DeepEns, in many cases, they struggle to match its performance (Ovadia et al., 2019). We note that while some recent works have studied GNN calibration, they focus on node classification settings (Hsu et al., 2022; Wang et al., 2021; Kang et al., 2022) and are not directly relevant to this work as they make assumptions that are only applicable to node classification tasks (e.g., proposing regularizers that rely upon on similarity to training nodes or neighborhood similarity).

3.2 STOCHASTIC CENTERING FOR UNCERTAINTY QUANTIFICATION

Recently, it was found that applying a (random) constant bias to vector-valued (and image) data leads to non-trivial changes in the resulting solution of a DNN (Thiagarajan et al., 2022). This behavior was attributed to the lack of shift-invariance in the neural tangent kernel (NTK) induced by conventional neural networks such as MLPs and CNNs. Building upon this observation, Thiagarajan et al. proposed a single model uncertainty estimation method, Δ -UQ, based on the principle of *anchoring*. Conceptually, anchoring is the process of creating a relative representation for an input sample x in terms of a random anchor c (which is used to perform the *stochastic centering*), $[x - c, c]$. By choosing different anchors randomly in each training iteration, Δ -UQ emulates the process of sampling different solutions from the hypothesis space (akin to an ensemble). During inference, Δ -

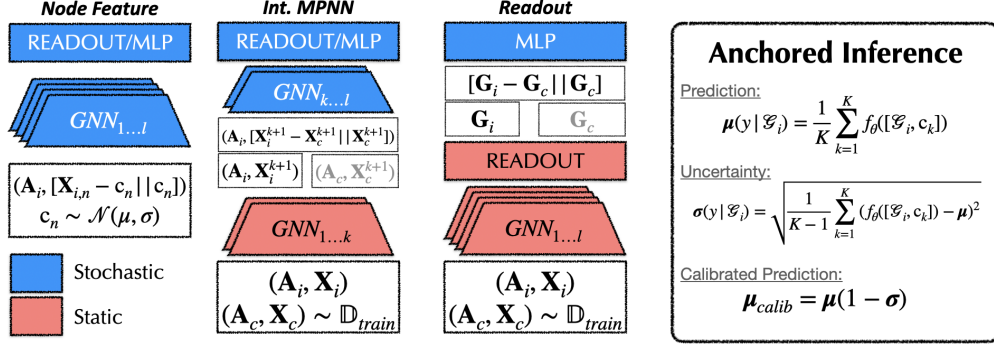


Figure 2: **Overview of G- Δ UQ.** We propose three different stochastic centering variants that induce varying levels of stochasticity in the underlying GNN. Notably, READOUT stochastic centering allows for using pretrained models with G- Δ UQ.

UQ aggregates multiple predictions obtained via different random anchors and produces uncertainty estimates. Formally, given a trained stochastically centered model, $f_{\theta} : [\mathbf{X} - \mathbf{C}, \mathbf{C}] \rightarrow \hat{\mathbf{Y}}$, let $\mathbf{C} := \mathbf{X}_{train}$ be the anchor distribution, $x \in \mathbf{X}_{test}$ be a test sample, and anchor $c \in \mathbf{C}$ be anchor. Then, the mean target class prediction, $\mu(y|x)$, and corresponding variance, $\sigma(y|x)$ over K random anchors are computed as:

$$\mu(y|x) = \frac{1}{K} \sum_{k=1}^K f_{\theta}([x - c_k, c_k]) \quad (4)$$

$$\sigma(y|x) = \sqrt{\frac{1}{K-1} \sum_{k=1}^K (f_{\theta}([x - c_k, c_k]) - \mu)^2} \quad (5)$$

Since the variance over K anchors captures epistemic uncertainty by sampling different hypotheses, these estimates can be used to modulate the predictions: $\mu_{calib} = \mu(1 - \sigma)$. The resulting calibrated predictions and uncertainty estimates have led to state-of-the-art performance on image outlier rejection and calibration tasks, while still only requiring a single model. Furthermore, it was separately shown that anchoring can also be used to improve the extrapolation behavior of DNNs (Netanyahu et al., 2023). However, while an attractive paradigm, there are several challenges to using stochastic centering with GNNs and graph data. We discuss and remedy these below in Sec. 4.

4 GRAPH- Δ UQ: UNCERTAINTY-BASED PREDICTION CALIBRATION

In this section, we introduce, G- Δ UQ, a novel single-model UQ method that helps improve the performance of CIs without sacrificing computational efficiency or accuracy by extending the recently proposed stochastic centering paradigm to graph data. (See Fig. 2 for an overview.)

As discussed in Sec. 3, the stochastic centering and anchoring paradigm has demonstrated significant promise in computer vision, yet there are several challenges that must be addressed prior to applying it to GNNs and graph data. Notably, previous research on stochastic centering has focused on traditional vision models (CNNs, ResNets, ViT) and relied on straightforward input space transformations (e.g., subtraction and channel-wise concatenation: $[\mathbf{X} - \mathbf{C}, \mathbf{C}]$) to construct anchored representations. However, graph datasets are structured, discrete, and variable-sized, where such trivial transformations do not exist. Moreover, the distribution shifts encountered in graph datasets exhibit distinct characteristics compared to those typically examined in the vision literature that must be accounted for when sampling the underlying GNN hypothesis space. Therefore, it is non-trivial to design anchors that are capable of appropriately capturing epistemic uncertainty.

Below, we discuss not only how to extend stochastic centering to GNNs and structured data, (G- Δ UQ), but also propose partially stochastic and pretrained variants that further improve the capabilities of anchored GNNs. In Section 5, we empirically demonstrate the advantages of our approach.

4.1 NODE FEATURE ANCHORING

Recall that in Δ -UQ, input samples are transformed into an anchored representation, by directly subtracting the input and anchor, and then concatenating them channel-wise, where the first DNN layer is correspondingly modified to accommodate the additional channels. While this is reasonable for vector-valued data or images, due to the variability graph size and discrete nature, performing a structural residual operation, $(\mathbf{A} - \mathbf{A}_c, \mathbf{A}_c)$ with respect to a graph sample, $\mathcal{G} = (\mathbf{X}, \mathbb{E}, \mathbf{A}, Y)$, and another anchor graph, $\mathcal{G}_c = (\mathbf{X}_c, \mathbb{E}_c, \mathbf{A}_c, Y_c)$, would introduce artificial edge weights and connectivity artifacts that can harm convergence. Likewise, we cannot *directly* anchor using the node features, \mathbf{X} , since the underlying graphs are different sizes, and a set of node features cannot be considered IID. To this end, we first create a distribution over the training dataset node features and sample anchors from this distribution as follows.

We first fit a Gaussian distribution $(\mathcal{N}(\mu, \sigma))$ to the training node features. Then, during training, we randomly sample an anchor for each node. Mathematically, given the anchor $\mathbf{C}^{N \times d} \sim \mathcal{N}(\mu, \sigma)$, we create the anchor/query node feature pair $[\mathbf{X}_i - \mathbf{C} \parallel \mathbf{X}_i]$, where \parallel denotes concatenation, and i is the node index. During inference, we sample a fixed set of K anchors and compute residuals for all nodes with respect to the same anchor, e.g., $\mathbf{c}^{1 \times d_k} \sim \mathcal{N}(\mu, \sigma) ([\mathbf{X}_i - \mathbf{c}_k \parallel \mathbf{X}_i])$, with appropriate broadcasting. For datasets with categorical node features, it is more beneficial to perform the anchoring operation after embedding the node features in a continuous space. Alternatively, considering the advantages of PEs in enhancing model expressivity (Wang et al., 2022b), one can compute positional information for each node and perform anchoring based on these encodings. While performing anchoring with respect to the node features is perhaps the most direct extension of Δ -UQ to graphs, as it results in a fully stochastically centered GNN, only using node features for anchoring neglects direct information about the underlying structure, which may lead to less diversity when sampling from the hypothesis space. Below, we introduce hidden layer variants that create partially stochastic GNNs that exploit message-passing to capture both feature and structural information during hypothesis sampling.

4.2 HIDDEN LAYER ANCHORING

While performing anchoring in the input space creates a fully stochastic neural network as all parameters are learned using the randomized input, it was recently demonstrated with respect to Bayesian neural networks that relaxing the assumption of fully stochastic to partially stochastic neural networks not only leads to strong computational benefits, but also may improve calibration (Sharma et al., 2023). Motivated by this observation, we extend G- Δ UQ to support anchoring in intermediate layers, in lieu of the input layer. This allows for *partially stochastic* GNNs, wherein the layers prior to the anchoring step are deterministic. Moreover, intermediate layer anchoring has the additional benefit that anchors will be able to sample hypotheses that consider both topological and node feature information due to MPNN steps, and supports using pretrained GNNs. We introduce these variants below. (See Fig. 2 for a visual representation.)

Intermediate MPNN Anchoring: Given a GNN containing ℓ MPNN layers, let $r \leq \ell$ be the layer at which we perform node feature anchoring. We obtain the anchor/sample pair by computing the intermediate node representations from the first r MPNN layers. We then randomly shuffle the node features over the entire *batch*, $(\mathbf{C} = \text{SHUFFLE}(\mathbf{X}_i^{r+1}))$, concatenate the residuals, and proceed with the READOUT and MLP layers as with the standard Δ -UQ model. Note that, we do not consider the gradients of the query sample when updating the parameters, and the MPNN^{r+1} layer is modified to accept inputs of dimension $d_r \times 2$ (to take in anchored representations as inputs). Another difference from the input space implementation is that we fix the set of anchors and subtract a single anchor from all node representations in an iteration (instead of sampling uniquely), e.g., $\mathbf{c}^{1 \times d} = \mathbf{X}_c^{r+1}[n, :]$ and $[\mathbf{X}_{i,n}^{r+1} - \mathbf{c} \parallel \mathbf{c}]$. This process is shown below, assume appropriate broadcasting:

$$\begin{aligned} \mathbf{X}^{r+1} &= \text{MPNN}^{1 \dots r} \\ \mathbf{X}^{r+1} &= \text{MPNN}^{r+1 \dots \ell}([\mathbf{X}^{r+1} - \mathbf{C}, \mathbf{X}^{r+1}], \mathbf{A}) \\ \hat{Y} &= \text{MLP}(\text{READOUT}(\mathbf{X}^{\ell+1})) \end{aligned}$$

Intermediate Read Out Anchoring: While READOUT anchoring is conceptually similar to intermediate MPNN anchoring, we now only obtain a different anchor for each hidden graph representation, instead of individual nodes. This allows us to sample hypotheses after all node information has been aggregated over ℓ hops. This is demonstrated below:

$$\mathbf{G} = \text{READOUT}(\mathbf{X}), \mathbf{G}_c = \text{READOUT}(\mathbf{X}_c)$$

$$\hat{Y} = \text{MLP}([\mathbf{G} - \mathbf{G}_c, \mathbf{G}_c])$$

Pretrained Anchoring: Lastly, we note that in order to be compatible with the stochastic centering framework (the input layer or chosen intermediate layer), the network architecture must be modified and retrained from scratch. To circumvent this, we consider a variant of READOUT anchoring using a pretrained GNN backbone. Here, the final MLP layer of a pretrained model is discarded, and reinitialized to accommodate query/anchor pairs. We then freeze the MPNN, and only train the anchored classifier head. This allows for an inexpensive, limited stochasticity GNN.

While all G- Δ UQ variants are able to sample from the underlying hypothesis space (see Fig. 10), each variant will provide somewhat different uncertainty estimates. Through our extensive evaluation, we show that the complexity of the task and the nature of the distribution shift will determine which of the variants is best suited and make some recommendations on which variants to use.

5 UNCERTAINTY-BASED PREDICTION CALIBRATION UNDER DISTRIBUTION SHIFT USING G- Δ UQ

In this section, we demonstrate the effectiveness of G- Δ UQ in improving the reliability of CIs on various tasks (calibration, generalization gap prediction and OOD detection) as well as various distribution shifts (size, covariate and concept).

5.1 SIZE GENERALIZATION

While GNNs are well-known to struggle when generalizing to larger size graphs (Buffelli et al., 2022; Yehudai et al., 2021; Chen et al., 2022), their predictive uncertainty behavior with respect to such shifts remains under studied. Given that such shifts can be expected at deployment, reliable uncertainty estimates under this setting are important for safety critical applications. We note that while sophisticated training strategies can be used to improve size generalization (Buffelli et al., 2022; Bevilacqua et al., 2021), our focus is primarily on the quality of uncertainty estimates, so we do not consider such techniques. However, we note that G- Δ UQ can be used in conjunction with such techniques.

Experimental Set-up. Following the procedure of (Buffelli et al., 2022; Yehudai et al., 2021), we create a size distribution shift by taking the smallest 50%-quantile of graph size for the training set, and reserving the larger quantiles (>50%) for evaluation. Unless, otherwise noted, we report results on the largest 10% quantile to capture performance on the largest shift. We utilize this splitting procedure on four well-known benchmark binary graph classification datasets from the TUDataset repository (Morris et al., 2020): D&D, NCI1, NCI109, and PROTEINS. (See App. A.3 for dataset statistics.) We further consider three different backbone GNN models, GCN (Kipf & Welling, 2017), GIN (Xu et al., 2019), and PNA (Corso et al., 2020). All models contain three message passing layers and the same sized hidden representation. The accuracy and expected calibration error on the larger-graph test set are reported for models trained with and without stochastic anchoring.

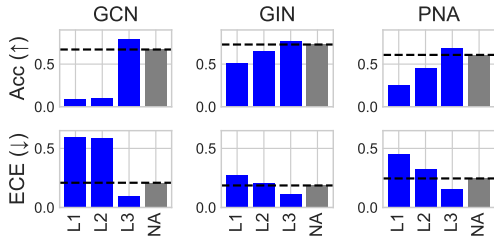


Figure 3: **Impact of Layer Selection on G- Δ UQ.** Performing anchoring at different layers leads the sampling of different hypothesis spaces. On D&D, we see that later layer anchoring corresponds to a better inductive bias and can lead to dramatically improved performance.

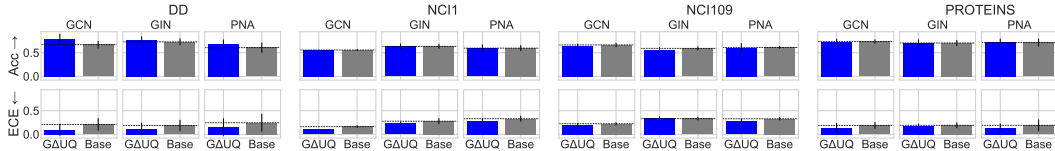


Figure 4: **Predictive Uncertainty under Size Distribution Shifts.** When evaluating the accuracy and calibration error of models trained with and without stochastic anchoring on dataset with a graph size distribution shift, we observe that stochastic centering decreases calibration error while improving or maintaining accuracy across datasets and different GNNs.

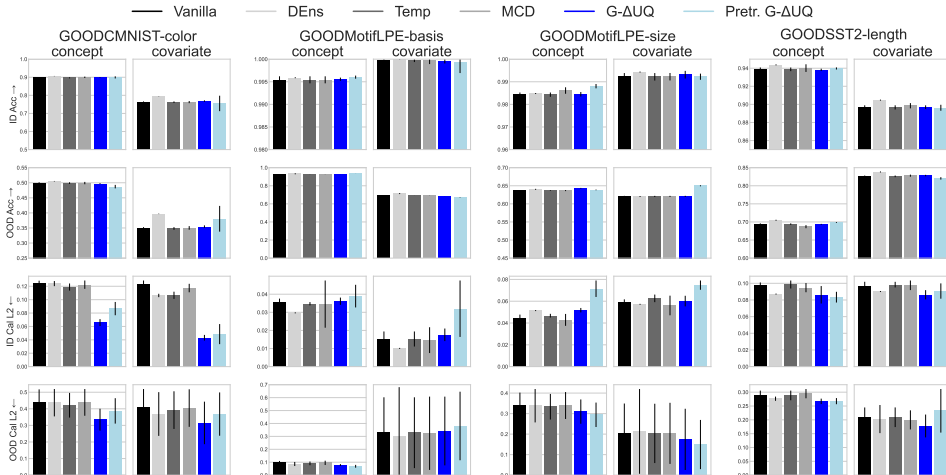


Figure 5: **Predictive Uncertainty under Concept and Covariate Shifts.** Stochastic anchoring leads to competitive in-distribution and out-of distribution test accuracy while improving calibration, across domains and shifts. This is particularly true when comparing to other single-model UQ methods.

Results. As noted in Sec. 4, stochastic anchoring can be applied at different layers, leading to the sampling of different hypothesis spaces and inductive biases. In order to empirically understand this behavior, we compare the performance of stochastic centering when applied at different layers on the D&D dataset, which comprises the most severe size shift from training to test set (see Fig. 3). We observe that applying stochastic anchoring after the READOUT layer (L3) dramatically improves both accuracy and calibration as the depth increases. While this behavior is less pronounced on other datasets (see Fig. 11), we find overall that applying stochastic anchoring at the last layer yields competitive performance on size generalization benchmarks and better convergence compared to stochastic centering performed at earlier layers.

Indeed, in Fig. 4, we compare the performance of last-layer anchoring against a non-anchored model on four datasets. We observe that G- Δ UQ improves calibration performance on most datasets, while generally maintaining or even improving the accuracy. Indeed, improvement is most pronounced on the largest shift (D&D), further emphasizing the benefits of stochastic centering.

5.2 EVALUATION UNDER CONCEPT AND COVARIATE SHIFTS

Here, we seek to understand the behavior of GNN CIs under controlled covariate and concept shifts, as well demonstrate the benefits of G- Δ UQ in providing reliable estimates under such shifts. Notably, we expand our evaluation beyond calibration error to include the safety-critical tasks of OOD detection (Hendrycks & Gimpel, 2017; Hendrycks et al., 2019) and generalization gap prediction tasks (Guillory et al., 2021; Ng et al., 2022; Trivedi et al., 2023a; Garg et al., 2022). We begin by introducing our data and additional tasks, and then present our results.

Experimental Set-up. In brief, concept shift corresponds to a change in the conditional distribution of labels given input from the training to evaluation datasets, while covariate shift corresponds to

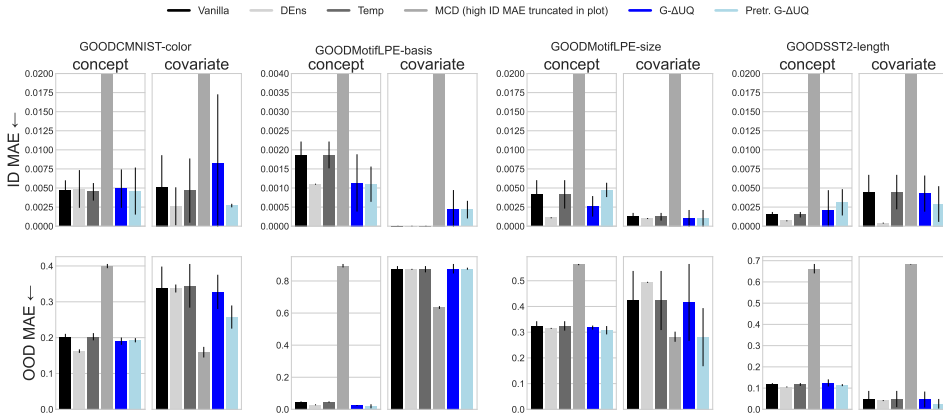


Figure 6: **Generalization Gap Prediction.** The mean absolute error when using scores obtained from different baselines in the challenging (and to the best of our knowledge, yet unexplored for graphs) task of generalization error prediction are reported. While there is not a dominant method, stochastic anchoring is very competitive, and yields among the lowest MAE of single-model UQ estimators. Notably, pretrained G- Δ UQ is particularly effective and outperforms the end-to-end variant.

change in the input distribution. We use the recently proposed Graph Out-Of Distribution (GOOD) benchmark (Gui et al., 2022) to obtain four different datasets (GOODCMNIST, GOODMotif-basis, GOODMotif-size, GOODSST2) with their corresponding in-/out- of distribution concept and covariate splits. To ensure fair comparison, we use the architectures and hyper-parameters suggested by the benchmark when training. Please see the supplementary for more details.

We consider the following baseline UQ methods in our analysis: Deep Ensembles (Lakshminarayanan et al., 2017), Monte Carlo Dropout (MCD) (Gal & Ghahramani, 2016), and our proposed G- Δ UQ, including the pretrained variant. DeepEnsembles is well known to be a highly performing baseline on uncertainty estimation tasks, but we emphasize that it requires training multiple models. This is in contrast to single model estimators, such as MCD and G- Δ UQ. We note that while MCD and G- Δ UQ can be applied at intermediate layers; we present results on the best performing layer but include the full results in the supplementary.

Using Confidence Estimates in Safety Critical Tasks. The safe deployment of graph machine learning models in critical applications requires that GNNs not only generalize to ID and OOD datasets, but that they do so safely. To this end, recent works (Hendrycks et al., 2022b; 2021; Trivedi et al., 2023b) have expanded model evaluation to include additional robustness metrics to provide a holistic view of model performance. Notably, while reliable confidence indicators are critical to success on these metrics, the impact of distributions shift on GNN confidence estimates remains under-explored. We introduce these additional tasks below.

Generalization Error Prediction: Accurate estimation of the expected generalization error on unlabeled datasets allows models with unacceptable performance to be pulled from production. To this end, generalization error predictors (GEPs) (Garg et al., 2022; Ng et al., 2022; Jiang et al., 2019; Trivedi et al., 2023a; Guillory et al., 2021) which assign sample-level scores, $S(x_i)$ which are then aggregated into dataset-level error estimates, have become popular. We use maximum softmax probability and a simple thresholding mechanism as the GEP (since we are interested in understanding the behavior of confidence indicators), and report the error between the predicted and true target dataset accuracy:

$$GEPError := \|\text{Acc}_{target} - \frac{1}{|X|} \sum_i \mathbb{I}(S(\bar{x}_i; F) > \tau)\|$$

where τ is tuned by minimizing GEP error on the validation dataset. We use the confidences obtained by the different baselines as sample-level scores, $S(x_i)$ corresponding to the model’s expectation that a sample is correct. The MAE between the estimated error and true error is reported on both in- and out-of -distribution test splits provided by the GOOD benchmark.

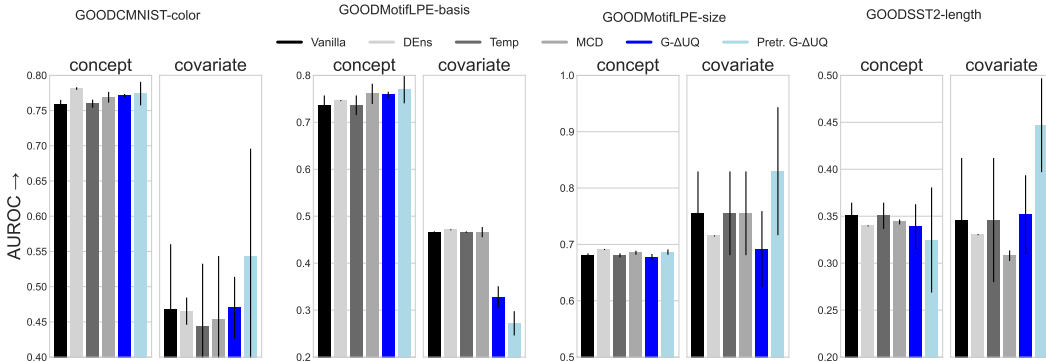


Figure 7: **OOD Detection.** The AUROC is reported for the task of detecting out-of-distribution samples. Under concept shift, the proposed G- Δ UQ variants are very competitive with other baselines, including DeepEnS. Under covariate shifts, except for GOODMotif-basis, pretrained G- Δ UQ produces significant improvements over all baselines, including end-to-end G- Δ UQ training.

Out-of-Distribution Detection: By reliably detecting OOD samples and abstaining from making predictions, models can avoid over extrapolating to distributions which are not relevant. While many scores have been proposed for detection (Hendrycks et al., 2019; 2022a; Lee et al., 2018; Wang et al., 2022a; Liu et al., 2020), flexible, popular baselines, such as maximum softmax probability and predictive entropy (Hendrycks & Gimpel, 2017), can be derived from confidence indicators relying upon prediction probabilities. Here, we report the AUROC for the binary classification task of detecting OOD samples using the maximum softmax probability (Kirchheim et al., 2022).

We briefly note that while more sophisticated scores can be used, our focus is on the reliability of GNN confidence indicators and thus we choose scores directly related to those estimates. Moreover, since sophisticated scores can often be derived from prediction probabilities, we expect their performance would also be improved with better estimates.

Results. We report the results in Figs. 5, 6, and 7. Our observations are below. Results are reported over three seeds.

Accuracy & Calibration. In Fig. 5, we observe that using stochastic anchoring via G- Δ UQ yields competitive accuracy, especially in comparison to other single-model methods such as MCD, temperature scaling, or the base GNN model: in-distribution accuracy is higher on 6 out of 8 dataset/shift combinations, and out-of-distribution accuracy is higher on 5 out of 8 combinations. While Deep Ensembles is the most accurate method on a majority of datasets, they are known to be computationally expensive. Moreover, the simpler stochastic anchoring procedure generally comes close to the accuracy of Deep Ensembles, and in a few cases (covariate shift on GOODCMNIST and GOODMotif-size datasets), can noticeably outperform it. Stochastic anchoring also excels in improving calibration, improving in-distribution calibration compared to all baselines on 4 out of 8 combinations. **Most importantly, out-of-distribution calibration error is decreased by stochastic anchoring on 7 of 8 dataset/shift combinations compared to all other methods (single-model or ensemble).**

Generalization Gap Prediction. Next, we study all of our methods on the GOOD benchmarks for the task of generalization gap prediction, and report the results in Fig. 6. On this challenging task, there is no clear winner across all benchmarks. However, G- Δ UQ variants are consistently competitive in MAE, and yield among the lowest MAE (across the board lower than other single-model UQ methods). In particular, **the pretrained G- Δ UQ variant produces on average the lowest MAE for generalization gap estimation.**

OOD Detection. Finally, we consider the task of detecting out-of-distribution samples. In Fig. 7, we see that the performance of stochastic anchoring methods under concept shift is generally very competitive with other UQ methods. For covariate shifts, except for the GOODMotif-basis dataset, stochastic anchoring produces high AUROC scores. In particular, on the GOODCMNIST-color, GOODSST2-length and GOODMotif-size benchmarks, the pretrained variant of G- Δ UQ produces significantly improved AUROC scores. Finally, on GOODMotif-basis, however, both have lower

AUROC than other baselines; we suspect the reason for this to be the inherent simplicity of this dataset and that G- Δ UQ was prone to shortcuts.

Overall, we find that G- Δ UQ performs competitively across several tasks and distributions shifts, validating our approach as an effective mechanism for producing reliable confidence indicators.

6 CONCLUSION

In this work, we take a closer look at confidence estimation under distribution shifts in the context of graph neural networks. We begin by demonstrating that techniques for improving GNN expressivity, such as transformer architectures and using positional encodings, do not necessarily improve the estimation performance on a simple structural distortion shift benchmark. To this end, we seek to improve the uncertainty estimation of GNNs by adapting the principle of stochastic anchoring for discrete, structured settings. We propose several G- Δ UQ variants, and demonstrate the benefits of partial stochasticity when estimating uncertainty. Our evaluation is extensive, spanning multiple types of distribution shift (size, concept, covariate) while considering multiple safety critical tasks that require reliable estimates (calibration, generalization gap prediction, and OOD detection.) The proposed G- Δ UQ improves estimation performance on a number of tasks, while remaining scalable. Overall, our paper rigorously studies uncertainty estimation for GNNs, identifies several shortcomings in existing approaches and proposes a flexible framework for reliable estimation. In future work, we will extend our framework to support link prediction and node classification tasks, as well as provide an automated mechanism for creating partially stochastic GNNs.

7 ACKNOWLEDGEMENTS

This work was performed under the auspices of the U.S. Department of Energy by the Lawrence Livermore National Laboratory under Contract No. DE-AC52-07NA27344, Lawrence Livermore National Security, LLC and is partially supported by the LLNL-LDRD Program under Project No. 2-ERD-006. This work is also partially supported by the National Science Foundation under CAREER Grant No. IIS 1845491, Army Young Investigator Award No. W9-11NF1810397, and Adobe, Amazon, Facebook, and Google faculty awards. Any opinions, findings, and conclusions or recommendations expressed here are those of the author(s) and do not reflect the views of funding parties. PT thanks Ekdeep Singh Lubana and Vivek Sivaraman for useful discussions during the course of this project.

REFERENCES

- Radhakrishna Achanta, Appu Shaji, Kevin Smith, Aurélien Lucchi, Pascal Fua, and Sabine Süsstrunk. SLIC superpixels compared to state-of-the-art superpixel methods. *IEEE Trans. Pattern Anal. Mach. Intell.*, 2012.
- Uri Alon and Eran Yahav. On the bottleneck of graph neural networks and its practical implications. In *Proc. Int. Conf. on Learning Representations (ICLR)*, 2021.
- Beatrice Bevilacqua, Yangze Zhou, and Bruno Ribeiro. Size-invariant graph representations for graph classification extrapolations. In *Proc. Int. Conf. on Machine Learning (ICML)*, 2021.
- Charles Blundell, Julien Cornebise, Koray Kavukcuoglu, and Daan Wierstra. Weight uncertainty in neural network. In *Proc. Int. Conf. on Machine Learning (ICML)*, 2015.
- Davide Buffelli, Pietro Liò, and Fabio Vandin. Sizeshiftreg: a regularization method for improving size-generalization in graph neural networks. In *Proc. Adv. in Neural Information Processing Systems (NeurIPS)*, 2022.
- Yongqiang Chen, Yonggang Zhang, Yatao Bian, Han Yang, Kaili Ma, Binghui Xie, Tongliang Liu, Bo Han, and James Cheng. Learning causally invariant representations for out-of-distribution generalization on graphs. In *Proc. Adv. in Neural Information Processing Systems (NeurIPS)*, 2022.
- Ching-Yao Chuang and Stefanie Jegelka. Tree mover’s distance: Bridging graph metrics and stability of graph neural networks. In *Proc. Adv. in Neural Information Processing Systems NeurIPS*, 2022.
- Gabriele Corso, Luca Cavalleri, Dominique Beaini, Pietro Liò, and Petar Velickovic. Principal neighbourhood aggregation for graph nets. In *NeurIPS*, 2020.
- Nicki Skafte Detlefsen, Jiri Borovec, Justus Schock, Ananya Harsh, Teddy Koker, Luca Di Liello, Daniel Stancl, Changsheng Quan, Maxim Grechkin, and William Falcon. Torchmetrics - measuring reproducibility in pytorch, 2022. URL <https://github.com/Lightning-AI/torchmetrics>.
- Mucong Ding, Kezhi Kong, Jiuhai Chen, John Kirchenbauer, Micah Goldblum, David Wipf, Furong Huang, and Tom Goldstein. A closer look at distribution shifts and out-of-distribution generalization on graphs. In *NeurIPS 2021 Workshop on Distribution Shifts: Connecting Methods and Applications*, 2021.
- Vijay Prakash Dwivedi, Chaitanya K. Joshi, Thomas Laurent, Yoshua Bengio, and Xavier Bresson. Benchmarking graph neural networks. *CoRR*, 2020.
- Vijay Prakash Dwivedi, Anh Tuan Luu, Thomas Laurent, Yoshua Bengio, and Xavier Bresson. Graph neural networks with learnable structural and positional representations. In *Proc. Int. Conf. on Learning Representations (ICLR)*, 2022a.
- Vijay Prakash Dwivedi, Ladislav Rampásek, Michael Galkin, Ali Parviz, Guy Wolf, Anh Tuan Luu, and Dominique Beaini. Long range graph benchmark. In *Proc. Adv. in Neural Information Processing Systems NeurIPS, Datasets and Benchmark Track*, 2022b.
- Yarin Gal and Zoubin Ghahramani. Dropout as a bayesian approximation: Representing model uncertainty in deep learning. In *Proc. Int. Conf. on Machine Learning (ICML)*, 2016.
- Saurabh Garg, Sivaraman Balakrishnan, Zachary C. Lipton, Behnam Neyshabur, and Hanie Sedghi. Leveraging unlabeled data to predict out-of-distribution performance. In *Proc. Int. Conf. on Learning Representations (ICLR)*, 2022.
- Thomas Gaudelot, Ben Day, Arian R. Jamasb, Jyothish Soman, Cristian Regep, Gertrude Liu, Jeremy B. R. Hayter, Richard Vickers, Charles Roberts, Jian Tang, David Roblin, Tom L. Blundell, Michael M. Bronstein, and Jake P. Taylor-King. Utilising graph machine learning within drug discovery and development. *CoRR*, abs/2012.05716, 2020.

- Shurui Gui, Xiner Li, Limei Wang, and Shuiwang Ji. GOOD: A graph out-of-distribution benchmark. In *Proc. Adv. in Neural Information Processing Systems (NeurIPS), Benchmark Track*, 2022.
- Devin Guillory, Vaishaal Shankar, Sayna Ebrahimi, Trevor Darrell, and Ludwig Schmidt. Predicting with confidence on unseen distributions. In *ICCV*, 2021.
- Chuan Guo, Geoff Pleiss, Yu Sun, and Kilian Q. Weinberger. On calibration of modern neural networks. In *Proc. of the Int. Conf. on Machine Learning, (ICML)*, 2017.
- Xiaoxin He, Bryan Hooi, Thomas Laurent, Adam Perold, Yann LeCun, and Xavier Bresson. A generalization of vit/mlp-mixer to graphs. *CoRR*, abs/2212.13350, 2022.
- Dan Hendrycks and Kevin Gimpel. A baseline for detecting misclassified and out-of-distribution examples in neural networks. In *Proc. Int. Conf. on Learning Representations (ICLR)*, 2017.
- Dan Hendrycks, Mantas Mazeika, and Thomas G. Dietterich. Deep anomaly detection with outlier exposure. In *Proc. Int. Conf. on Learning Representations (ICLR)*, 2019.
- Dan Hendrycks, Nicholas Carlini, John Schulman, and Jacob Steinhardt. Unsolved problems in ML safety. *CoRR*, abs/2109.13916, 2021.
- Dan Hendrycks, Steven Basart, Mantas Mazeika, Andy Zou, Joseph Kwon, Mohammadreza Mostajabi, Jacob Steinhardt, and Dawn Song. Scaling out-of-distribution detection for real-world settings. In *Proc. Int. Conf. on Machine Learning (ICML)*, 2022a.
- Dan Hendrycks, Andy Zou, Mantas Mazeika, Leonard Tang, Bo Li, Dawn Song, and Jacob Steinhardt. Pixmix: Dreamlike pictures comprehensively improve safety measures. In *Proc. Int. Conf. on Computer Vision and Pattern Recognition (CVPR)*, 2022b.
- Hans Hao-Hsun Hsu, Yuesong Shen, Christian Tomani, and Daniel Cremers. What makes graph neural networks miscalibrated? In *Proc. Adv. in Neural Information Processing Systems NeurIPS*, 2022.
- Yiding Jiang, Dilip Krishnan, Hossein Mobahi, and Samy Bengio. Predicting the generalization gap in deep networks with margin distributions. In *7th International Conference on Learning Representations, ICLR 2019, New Orleans, LA, USA, May 6-9, 2019*. OpenReview.net, 2019.
- Jian Kang, Qinghai Zhou, and Hanghang Tong. Jurygen: Quantifying jackknife uncertainty on graph convolutional networks. In *Proc. Int. Conf. on Knowledge Discovery & Data Mining, KDD*, 2022.
- Thomas N Kipf and Max Welling. Semi-supervised classification with graph convolutional networks. In *ICLR*, 2017.
- Konstantin Kirchheim, Marco Filax, and Frank Ortmeier. Pytorch-ood: A library for out-of-distribution detection based on pytorch. In *Workshop at the Proc. Int. Conf. on Computer Vision and Pattern Recognition CVPR*, 2022.
- Boris Knyazev, Graham W. Taylor, and Mohamed R. Amer. Understanding attention and generalization in graph neural networks. In *Proc. Adv. in Neural Information Processing Systems (NeurIPS)*, 2019.
- Ananya Kumar, Percy Liang, and Tengyu Ma. Verified uncertainty calibration. In *Proc. Adv. in Neural Information Processing Systems NeurIPS*, 2019.
- Balaji Lakshminarayanan, Alexander Pritzel, and Charles Blundell. Simple and scalable predictive uncertainty estimation using deep ensembles. In *Proc. Adv. in Neural Information Processing Systems (NeurIPS)*, 2017.
- Kimin Lee, Kibok Lee, Honglak Lee, and Jinwoo Shin. A simple unified framework for detecting out-of-distribution samples and adversarial attacks. In *Proc. Adv. in Neural Information Processing Systems NeurIPS*, 2018.
- Pan Li, Yanbang Wang, Hongwei Wang, and Jure Leskovec. Distance encoding: Design provably more powerful neural networks for graph representation learning. In *Proc. Adv. in Neural Information Processing Systems NeurIPS*, 2020.

- Weitang Liu, Xiaoyun Wang, John D. Owens, and Yixuan Li. Energy-based out-of-distribution detection. In *Proc. Adv. in Neural Information Processing Systems NeurIPS*, 2020.
- Matthias Minderer, Josip Djolonga, Rob Romijnders, Frances Hubis, Xiaohua Zhai, Neil Houlsby, Dustin Tran, and Mario Lucic. Revisiting the calibration of modern neural networks. In *Proc. Adv. in Neural Information Processing Systems (NeurIPS)*, 2021.
- Christopher Morris, Nils M. Kriege, Franka Bause, Kristian Kersting, Petra Mutzel, and Marion Neumann. Tudataset: A collection of benchmark datasets for learning with graphs. In *ICML 2020 Workshop on Graph Representation Learning and Beyond (GRL+ 2020)*, 2020. URL www.graphlearning.io.
- Luis Müller, Mikhail Galkin, Christopher Morris, and Ladislav Rampásek. Attending to graph transformers. *CoRR*, abs/2302.04181, 2023.
- Mahdi Pakdaman Naeini, Gregory F. Cooper, and Milos Hauskrecht. Obtaining well calibrated probabilities using bayesian binning. In *Proc. Conf. on Adv. of Artificial Intelligence (AAAI)*, 2015.
- Aviv Netanyahu, Abhishek Gupta, Max Simchowitz, Kaiqing Zhang, and Pulkit Agrawal. Learning to extrapolate: A transductive approach. In *Proc. Int. Conf. on Learning Representations (ICLR)*, 2023.
- Nathan Ng, Neha Hulkund, Kyunghyun Cho, and Marzyeh Ghassemi. Predicting out-of-domain generalization with local manifold smoothness. *CoRR*, abs/2207.02093, 2022.
- Yaniv Ovadia, Emily Fertig, Jie Ren, Zachary Nado, D. Sculley, Sebastian Nowozin, Joshua Dillon, Balaji Lakshminarayanan, and Jasper Snoek. Can you trust your model’s uncertainty? evaluating predictive uncertainty under dataset shift. In *Proc. Adv. in Neural Information Processing Systems NeurIPS*, 2019.
- Ladislav Rampásek, Mikhail Galkin, Vijay Prakash Dwivedi, Anh Tuan Luu, Guy Wolf, and Dominique Beaini. Recipe for a General, Powerful, Scalable Graph Transformer. In *Proc. Adv. in Neural Information Processing Systems (NeurIPS)*, 2022.
- Mrinank Sharma, Sebastian Farquhar, Eric Nalisnick, and Tom Rainforth. Do bayesian neural networks need to be fully stochastic? In *AISTATS*, 2023.
- Jayaraman J. Thiagarajan, Rushil Anirudh, Vivek Narayanaswamy, and Peer-Timo Bremer. Single model uncertainty estimation via stochastic data centering. In *Proc. Adv. in Neural Information Processing Systems (NeurIPS)*, 2022.
- Jake Topping, Francesco Di Giovanni, Benjamin Paul Chamberlain, Xiaowen Dong, and Michael M. Bronstein. Understanding over-squashing and bottlenecks on graphs via curvature. In *Proc. Int. Conf. on Learning Representations ICLR*, 2022.
- Puja Trivedi, Danai Koutra, and Jayaraman J. Thiagarajan. A closer look at scoring functions and generalization prediction. In *ICASSP 2023-2023 IEEE International Conference on Acoustics, Speech and Signal Processing (ICASSP)*, pp. 1–5. IEEE, 2023a.
- Puja Trivedi, Danai Koutra, and Jayaraman J. Thiagarajan. A closer look at model adaptation using feature distortion and simplicity bias. In *Proc. Int. Conf. on Learning Representations (ICLR)*, 2023b.
- Petar Velickovic, Guillem Cucurull, Arantxa Casanova, Adriana Romero, Pietro Liò, and Yoshua Bengio. Graph attention networks. In *ICLR*, 2018.
- Haoqi Wang, Zhizhong Li, Litong Feng, and Wayne Zhang. Vim: Out-of-distribution with virtual-logit matching. In *Proc. Int. Conf. on Computer Vision and Pattern Recognition (CVPR)*, 2022a.
- Haorui Wang, Haoteng Yin, Muhan Zhang, and Pan Li. Equivariant and stable positional encoding for more powerful graph neural networks. In *Proc. Int. Conf. on Learning Representations (ICLR)*, 2022b.

- Xiao Wang, Hongrui Liu, Chuan Shi, and Cheng Yang. Be confident! towards trustworthy graph neural networks via confidence calibration. In *Proc. Adv. in Neural Information Processing Systems NeurIPS*, 2021.
- Olivia Wiles, Sven Gowal, Florian Stimberg, Sylvestre-Alvise Rebuffi, Ira Ktena, Krishnamurthy Dj Dvijotham, and Ali Taylan Cemgil. A Fine-Grained Analysis on Distribution Shift. In *Proc. Int. Conf. on Learning Representations (ICLR)*, 2022.
- Keyulu Xu, Weihua Hu, Jure Leskovec, and Stefanie Jegelka. How powerful are graph neural networks? In *ICLR*, 2019.
- Keyulu Xu, Mozhi Zhang, Stefanie Jegelka, and Kenji Kawaguchi. Optimization of graph neural networks: Implicit acceleration by skip connections and more depth. In *Proc. Int. Conf. on Machine Learning (ICML)*, 2021.
- Yujun Yan, Jiong Zhu, Marlena Duda, Eric Solarz, Chandra Sekhar Sripada, and Danai Koutra. Groupinn: Grouping-based interpretable neural network for classification of limited, noisy brain data. In *Proc. Int. Conf. on Knowledge Discovery & Data Mining, KDD*, 2019.
- Jianwei Yang, Jiasen Lu, Stefan Lee, Dhruv Batra, and Devi Parikh. Graph R-CNN for scene graph generation. In *Proc. Euro. Conf. on Computer Vision (ECCV)*, 2018.
- Gilad Yehudai, Ethan Fetaya, Eli Meir, Gal Chechik, and Haggai Maron. From local structures to size generalization in graph neural networks. In *International Conference on Machine Learning*, pp. 11975–11986. PMLR, 2021.
- Muhan Zhang and Yixin Chen. Link prediction based on graph neural networks. In *Proc. Adv. in Neural Information Processing Systems NeurIPS*, 2018.
- Lingxiao Zhao, Wei Jin, Leman Akoglu, and Neil Shah. From stars to subgraphs: Uplifting any GNN with local structure awareness. In *Proc. Int. Conf. on Learning Representations (ICLR)*, 2022.
- Yanqiao Zhu, Yuanqi Du, Yinkai Wang, Yichen Xu, Jieyu Zhang, Qiang Liu, and Shu Wu. A survey on deep graph generation: Methods and applications. In *Learning on Graphs Conference (LoG)*, 2022.

A APPENDIX

A.1 DETAILS ON SUPER-PIXEL EXPERIMENTS

We provide an example of the rotated images and corresponding super-pixel graphs in Fig. 8, as well as additional resulting using the GINE backbone.

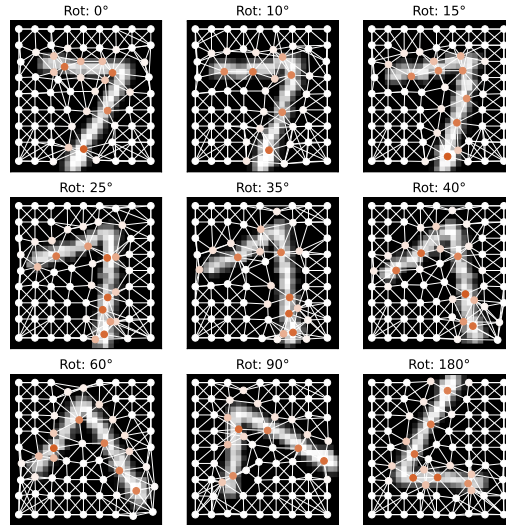


Figure 8: **Rotated Super-pixel MNIST.** Rotating images prior to creating super-pixels to leads to some structural distortion [Ding et al.](#). We can see that the class-discriminative information is preserved, despite rotation. This allows for simulating different levels of distribution shifts, while still ensuring that samples are valid.

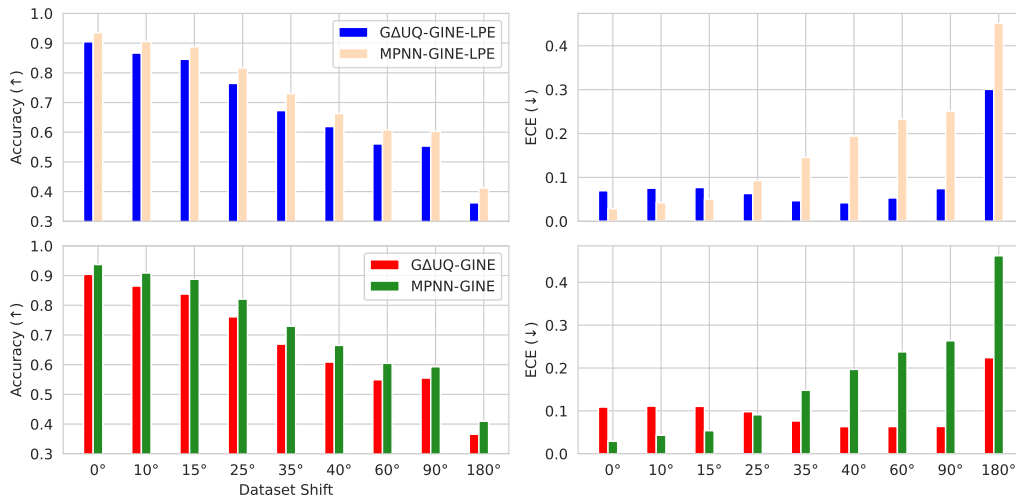


Figure 9: **Rotated Super-pixel MNIST, GINE Backbone.** We report additional results for performance on rotated-superpixel MNIST using a GINE backbone and READOUT stochastic anchoring. While G- Δ UQ does lose some accuracy, we see at higher levels of distortion, that it is significantly better calibrated.

A.2 STOCHASTIC CENTERING ON THE EMPRICAL NTK OF GRAPH NEURAL NETWORKS

Using a simple grid-graph dataset and 4 layer GIN model, we compute the Fourier spectrum of the NTK. As shown in Fig. 10, we find that shifts to the node features can induce systematic changes to the spectrum.

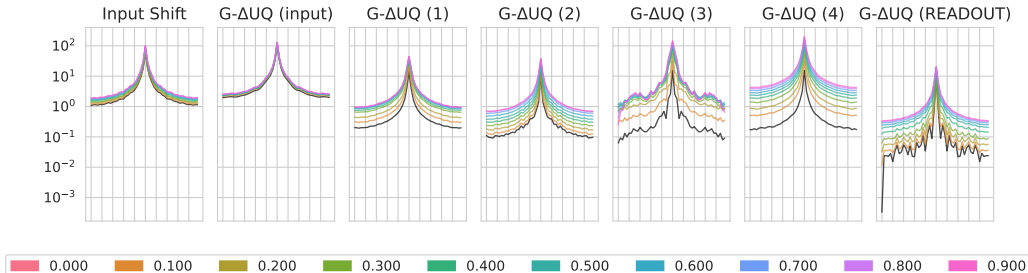


Figure 10: **Stochastic Centering with the empirical GNN NTK.** We find that performing constant shifts at intermediate layers introduces changes to a GNN’s NTK. We include a vanilla GNN NTK in black for reference. Further, note the shape of the spectrum should not be compared across subplots as each subplot was created with a different random initialization.

A.3 DATASET STATISTICS

The statistics for the size generalization experiments (see Sec. 5.1) are provided below in Table 1.

Table 1: **Size Generalization Dataset Statistics:** This table is directly reproduced from (Buffelli et al., 2022), who in turn used statistics from (Yehudai et al., 2021; Bevilacqua et al., 2021).

	NCII			NCII09		
	ALL	SMALLEST 50%	LARGEST 10%	ALL	SMALLEST 50%	LARGEST 10%
CLASS A	49.95%	62.30%	19.17%	49.62%	62.04%	21.37%
CLASS B	50.04%	37.69%	80.82%	50.37%	37.95%	78.62%
# OF GRAPHS	4110	2157	412	4127	2079	421
AVG GRAPH SIZE	29	20	61	29	20	61

	PROTEINS			DD		
	ALL	SMALLEST 50%	LARGEST 10%	ALL	SMALLEST 50%	LARGEST 10%
CLASS A	59.56%	41.97%	90.17%	58.65%	35.47%	79.66%
CLASS B	40.43%	58.02%	9.82%	41.34%	64.52%	20.33%
# OF GRAPHS	1113	567	112	1178	592	118
AVG GRAPH SIZE	39	15	138	284	144	746

A.4 LAYER SELECTION SIZE GENERALIZATION

As discussed in Sec. 5.1, the choice of anchoring layer can have a disparate effect on the accuracy and calibration of a dataset. For example, in Fig. 11, we see that while the choice of layer is very influential for DD, it is significantly less important for the other datasets. However, overall, we see that anchoring after READOUT leads to good performance.

A.5 GOOD BENCHMARK EXPERIMENTAL DETAILS

For our experiments in Sec. 5.2, we utilize the in/out-of-distribution covariate and concept splits provided by Gui et al. (2022). Furthermore, we use the suggested models and architectures provided by their package. In brief, we use GIN models with virtual nodes (except for GOODMotif) for training, and average scores over 3 seeds. When performing stochastic anchoring at a particular layer, we double the hidden representation size for that layer. Subsequent layers retain the original size of the vanilla model.

We use 10 samples when computing uncertainties using Monte Carlo Dropout, and manually set individual layers to “train” in order to perform layer-wise dropout. When performing stochastic

Table 4: **RotMNIST-Calibration.** Here, we report expanded results (calibration) on the Rotated MNIST dataset, including a variant that combines G- Δ UQ with Deep Ens. Notably, we see that anchored ensembles outperform basic ensembles in both accuracy and calibration.

MODEL	G- Δ UQ	LPE?	Avg.ECE (\downarrow)	ECE (10) (\downarrow)	ECE (15) (\downarrow)	ECE (25) (\downarrow)	ECE (35) (\downarrow)	ECE (40) (\downarrow)	ECE (60) (\downarrow)	ECE (90) (\downarrow)	ECE (180) (\downarrow)
GatecGCN	✓	✗	0.03778 ± 0.0015	0.05862 ± 0.0012	0.06804 ± 0.3402	0.12622 ± 0.0085	0.19502 ± 0.0118	0.24554 ± 0.0109	0.3011 ± 0.01314	0.3033 ± 0.01035	0.4896 ± 0.0132
GatecGCN-TEMP	✓	✗	0.0181 ± 0.00847	0.02924 ± 0.0129	0.03274 ± 0.1637	0.06878 ± 0.0335	0.1167 ± 0.04773	0.16182 ± 0.0666	0.2131 ± 0.08991	0.2228 ± 0.0755	0.38428 ± 0.0586
GatecGCN-DENS	✓	✗	0.03488 ± 0.00155	0.05434 ± 0.00205	0.0624 ± 0.002965	0.11856 ± 0.00666	0.18548 ± 0.00595	0.23334 ± 0.00851	0.28842 ± 0.01233	0.2915 ± 0.010884	-
GatecGCN-DENS	✓	✗	0.02574 ± 0.00027	0.03794 ± 0.00157	0.04254 ± 0.00115	0.08418 ± 0.00226	0.13482 ± 0.00103	0.18492 ± 0.00280	0.2375 ± 0.001238	0.2594 ± 0.00179	-
GatecGCN-DENS	✓	✗	0.01458 ± 0.00324	0.0185 ± 0.005383	0.02094 ± 0.00503	0.03638 ± 0.01210	0.06902 ± 0.03249	0.11416 ± 0.05638	0.16408 ± 0.07113	0.1664 ± 0.055580	-
GatecGCN	✓	✓	0.0364 ± 0.00305	0.05882 ± 0.0025	0.06804 ± 0.3402	0.12512 ± 0.0059	0.19148 ± 0.0070	0.2399 ± 0.00766	0.29732 ± 0.0087	0.30304 ± 0.0152	0.4863 ± 0.00851
GatecGCN-Temp	✓	✓	0.0218 ± 0.00673	0.02856 ± 0.0140	0.03386 ± 0.1693	0.06246 ± 0.0223	0.10884 ± 0.0187	0.14068 ± 0.0191	0.17554 ± 0.0214	0.1971 ± 0.04935	0.3264 ± 0.05404
GatecGCN-DENS	✓	✓	0.03316 ± 0.0023	0.0531 ± 0.00185	0.0614 ± 0.00433	0.1161 ± 0.00506	0.17878 ± 0.0059	0.22476 ± 0.0049	0.28026 ± 0.0071	0.28656 ± 0.0135	-
GatecGCN-DENS	✓	✓	0.02576 ± 0.0007	0.03784 ± 0.0010	0.0426 ± 0.00184	0.08308 ± 0.0012	0.13894 ± 0.0038	0.18988 ± 0.0025	0.2371 ± 0.00228	0.24934 ± 0.0053	-
GatecGCN-DENS	✓	✓	0.01686 ± 0.0024	0.02406 ± 0.0055	0.0274 ± 0.00766	0.02976 ± 0.0042	0.0364 ± 0.01213	0.0587 ± 0.03265	0.08836 ± 0.0429	0.11634 ± 0.0310	-
GPS	✓	✓	0.026 ± 0.0013	0.0437 ± 0.0009	0.0519 ± 0.1559	0.1076 ± 0.0057	0.1974 ± 0.0124	0.2727 ± 0.0084	0.3657 ± 0.0169	0.4336 ± 0.0236	0.5391 ± 0.0247
GPS (Pretrained)	✓	✓	0.0221 ± 0.0013	0.037 ± 0.0055	0.0442 ± 0.1327	0.0907 ± 0.0084	0.1649 ± 0.0183	0.2387 ± 0.0178	0.3347 ± 0.0268	0.4013 ± 0.0539	0.4771 ± 0.0222
GPS-TEMP	✓	✓	0.0207 ± 0.0013	0.0323 ± 0.0028	0.0386 ± 0.1159	0.0827 ± 0.0019	0.1531 ± 0.0072	0.2169 ± 0.0121	0.2906 ± 0.0164	0.3320 ± 0.0257	0.4648 ± 0.0643
GPS-DENS	✓	✓	0.02443 ± 0.0008	0.04113 ± 0.001	0.0486 ± 0.00059	0.10163 ± 0.00624	0.1878 ± 0.01192	0.26973 ± 0.00822	0.35656 ± 0.01544	0.417 ± 0.022351	-
GPS-DENS	✓	✓	0.0163 ± 0.0012	0.026 ± 0.0022	0.0298 ± 0	0.0658 ± 0	0.1233 ± 0	0.1952 ± 0	0.2747 ± 0	0.3438 ± 0	-
GPS-DENS	✓	✓	0.01425 ± 0.00014	0.0233 ± 0.00199	0.027425 ± 0.003	0.05505 ± 0.0041	0.10325 ± 0.0056	0.16435 ± 0.0060	0.243775 ± 0.00575	0.319925 ± 0.00235	-

Table 5: **GOODCMNIST-color, shifttype: concept**

Method	ID Acc	OOD Acc	ID Cal	OOD Cal
Vanilla	89.66 ± 0.28	49.88 ± 0.28	0.1241 ± 0.0042	0.4392 ± 0.0779
Dens	90.64 ± 0.08	50.51 ± 0.08	0.1240 ± 0.0038	0.4368 ± 0.0825
Temp	89.66 ± 0.28	49.88 ± 0.28	0.1189 ± 0.0053	0.4215 ± 0.0744
MCD	89.96 ± 0.39	49.89 ± 0.39	0.1224 ± 0.0062	0.4387 ± 0.0806
G- Δ UQ	89.88 ± 0.15	49.73 ± 0.15	0.0658 ± 0.0051	0.3343 ± 0.0660
Pretr. G- Δ UQ	89.92 ± 0.58	48.71 ± 0.58	0.0867 ± 0.0099	0.3874 ± 0.0766

Table 6: **GOODCMNIST-color, shifttype: covariate**

Method	ID Acc	OOD Acc	ID Cal	OOD Cal
Vanilla	76.19 ± 0.44	34.84 ± 0.44	0.1846 ± 0.0071	0.5507 ± 0.1473
Dens	79.36 ± 0.07	39.68 ± 0.07	0.1583 ± 0.0038	0.4954 ± 0.1773
Temp	76.19 ± 0.44	34.84 ± 0.44	0.1587 ± 0.0080	0.5271 ± 0.1526
MCD	76.27 ± 0.59	35.02 ± 0.59	0.1749 ± 0.0094	0.5437 ± 0.1522
G- Δ UQ	76.83 ± 0.41	35.46 ± 0.41	0.0643 ± 0.0063	0.4233 ± 0.1723
Pretr. G- Δ UQ	75.52 ± 4.27	38.05 ± 4.27	0.0724 ± 0.0223	0.4949 ± 0.1755

Table 7: **GOODMotifLPE-basis, shifttype: concept**

Method	ID Acc	OOD Acc	ID Cal	OOD Cal
Vanilla	99.54 ± 0.08	92.52 ± 0.08	0.0356 ± 0.0020	0.0954 ± 0.0144
Dens	99.59 ± 0.00	93.24 ± 0.00	0.0297 ± 0.00033	0.0863 ± 0.0158
Temp	99.54 ± 0.08	92.52 ± 0.08	0.0347 ± 0.0009	0.0910 ± 0.0143
MCD	99.54 ± 0.08	92.52 ± 0.08	0.0345 ± 0.0130	0.0951 ± 0.0167
G- Δ UQ	99.56 ± 0.04	92.54 ± 0.04	0.0361 ± 0.0020	0.0781 ± 0.0074
Pretr. G- Δ UQ	99.60 ± 0.03	93.63 ± 0.03	0.0389 ± 0.0063	0.0686 ± 0.0109

Table 8: **GOODMotifLPE-basis, shifttype: covariate**

Method	ID Acc	OOD Acc	ID Cal	OOD Cal
Vanilla	99.98 ± 0.04	69.08 ± 0.04	0.0161 ± 0.0044	0.3286 ± 0.2741
Dens	100.00 ± 0.00	71.37 ± 0.00	0.0106 ± 0.0001	0.2980 ± 0.3831
Temp	99.98 ± 0.04	69.08 ± 0.04	0.0161 ± 0.0044	0.3286 ± 0.2741
MCD	99.98 ± 0.09	69.13 ± 0.09	0.0154 ± 0.0075	0.3241 ± 0.2838
G- Δ UQ	99.96 ± 0.05	68.16 ± 0.05	0.0185 ± 0.0037	0.3417 ± 0.2661
Pretr. G- Δ UQ	99.92 ± 0.23	66.95 ± 0.23	0.0337 ± 0.0164	0.3806 ± 0.2653

Table 9: GOODMotifLPE-size, shifttype: concept

Method	ID Acc	OOD Acc	ID Cal	OOD Cal
Vanilla	98.43 ± 0.10	63.66 ± 0.10	0.0446 ± 0.0031	0.3401 ± 0.0622
Dens	98.48 ± 0.00	64.02 ± 0.00	0.0514 ± 0.0000	0.3384 ± 0.0814
Temp	98.43 ± 0.10	63.66 ± 0.10	0.0467 ± 0.0017	0.3335 ± 0.0623
MCD	98.61 ± 0.14	63.67 ± 0.14	0.0429 ± 0.0055	0.3394 ± 0.0656
G-ΔUQ	98.45 ± 0.10	64.31 ± 0.10	0.0518 ± 0.0020	0.3097 ± 0.0592
Pretr. G-ΔUQ	98.80 ± 0.10	63.86 ± 0.10	0.0714 ± 0.0075	0.2942 ± 0.0596

Table 10: GOODMotifLPE-size, shifttype: covariate

Method	ID Acc	OOD Acc	ID Cal	OOD Cal
Vanilla	99.22 ± 0.17	62.05 ± 0.17	0.0496 ± 0.0021	0.3527 ± 0.2483
Dens	99.43 ± 0.00	62.02 ± 0.00	0.0479 ± 0.0000	0.3671 ± 0.3557
Temp	99.22 ± 0.17	62.05 ± 0.17	0.0525 ± 0.0029	0.3504 ± 0.2489
MCD	99.22 ± 0.17	62.05 ± 0.17	0.0470 ± 0.0075	0.3507 ± 0.2564
G-ΔUQ	99.31 ± 0.17	62.06 ± 0.17	0.0504 ± 0.0041	0.3002 ± 0.2569
Pretr. G-ΔUQ	99.22 ± 0.14	65.00 ± 0.14	0.0626 ± 0.0036	0.2569 ± 0.2064

Table 11: GOODSST2-length, shifttype: concept

Method	ID Acc	OOD Acc	ID Cal	OOD Cal
Vanilla	93.88 ± 0.20	69.40 ± 0.20	0.0976 ± 0.0034	0.2882 ± 0.0175
Dens	94.37 ± 0.00	70.47 ± 0.00	0.0871 ± 0.001	0.2764 ± 0.0076
Temp	93.88 ± 0.20	69.40 ± 0.20	0.0986 ± 0.0048	0.2882 ± 0.0175
MCD	94.01 ± 0.42	68.69 ± 0.42	0.0948 ± 0.0055	0.2947 ± 0.0168
G-ΔUQ	93.82 ± 0.13	69.34 ± 0.13	0.0862 ± 0.0105	0.2668 ± 0.0098
Pretr. G-ΔUQ	93.97 ± 0.12	69.85 ± 0.12	0.0834 ± 0.0064	0.2676 ± 0.0111

Table 12: GOODSST2-length, shifttype: covariate

Method	ID Acc	OOD Acc	ID Cal	OOD Cal
Vanilla	89.67 ± 0.23	82.60 ± 0.23	0.1230 ± 0.0060	0.1590 ± 0.0269
Dens	90.47 ± 0.00	83.81 ± 0.00	0.1142 ± 0.0003	0.1540 ± 0.0386
Temp	89.67 ± 0.23	82.60 ± 0.23	0.1247 ± 0.0043	0.1590 ± 0.0270
MCD	89.85 ± 0.29	82.79 ± 0.29	0.1237 ± 0.0073	0.1517 ± 0.0262
G-ΔUQ	89.69 ± 0.20	82.82 ± 0.20	0.1093 ± 0.0070	90.1351 ± 0.0314
Pretr. G-ΔUQ	89.63 ± 0.33	82.04 ± 0.33	0.1150 ± 0.0116	0.1767 ± 0.0598

Table 13: GOOD-Datasets, OOD Detection Performance

Method	CMNIST (Color)		MotifLPE (Basis)		MotifLPE (Size)		SST2	
	Concept	Covariate	Concept	Covariate	Concept	Covariate	Concept	Covariate
Vanilla	0.7590 ± 0.0062	0.4682 ± 0.0920	0.7362 ± 0.0210	0.4662 ± 0.0015	0.6806 ± 0.0035	0.7552 ± 0.0743	0.3505 ± 0.0140	0.3459 ± 0.0661
Dens	0.7813 ± 0.0018	0.4652 ± 0.0193	0.7462 ± 0.0000	0.4711 ± 0.0000	0.6909 ± 0.0000	0.7151 ± 0.0000	0.3397 ± 0.0000	0.3304 ± 0.0000
Temp	0.7597 ± 0.0057	0.4443 ± 0.0883	0.7362 ± 0.0210	0.4662 ± 0.0015	0.6806 ± 0.0035	0.7552 ± 0.0743	0.3505 ± 0.0140	0.3459 ± 0.0661
MCD	0.7689 ± 0.0077	0.4536 ± 0.0900	0.7605 ± 0.0216	0.4662 ± 0.0108	0.6852 ± 0.0036	0.7552 ± 0.0743	0.3439 ± 0.0027	0.3080 ± 0.0056
G-ΔUQ	0.7711 ± 0.0024	0.4700 ± 0.0439	0.7585 ± 0.0065	0.3281 ± 0.0228	0.6774 ± 0.0055	0.6916 ± 0.0675	0.3389 ± 0.0239	0.3513 ± 0.0423
Pretr. G-ΔUQ	0.7741 ± 0.0167	0.5433 ± 0.1526	0.7694 ± 0.0290	0.2720 ± 0.0258	0.6864 ± 0.0047	0.8299 ± 0.1135	0.3247 ± 0.0559	0.4469 ± 0.0489

Table 14: GOODCMNIST-color, shifttype: concept, GenGap Performance

Method	ID MAE(↓)	OOD MAE(↓)
Vanilla	0.0047 ± 0.0013	0.2008 ± 0.0098
Dens	0.0049 ± 0.0025	0.1624 ± 0.0050
Temp	0.0045 ± 0.0011	0.2026 ± 0.0101
MCD	0.8966 ± 0.0021	0.3997 ± 0.0059
G-ΔUQ	0.0049 ± 0.0025	0.1901 ± 0.0102
Pretr. G-ΔUQ	0.0046 ± 0.0031	0.1928 ± 0.0058

Table 15: GOODCMNIST-color, shifttype: covariate, GenGap Performance

Method	ID MAE(↓)	OOD MAE(↓)
Vanilla	0.0051 ± 0.0042	0.5104 ± 0.0893
Dens	0.0026 ± 0.0025	0.5076 ± 0.0167
Temp	0.0047 ± 0.0042	0.5189 ± 0.0918
MCD	0.7598 ± 0.0031	0.2401 ± 0.0223
G-ΔUQ	0.0082 ± 0.0091	0.4933 ± 0.0721
Pretr. G-ΔUQ	0.0027 ± 0.0002	0.3877 ± 0.0486

Table 16: GOODMotifLPE-basis, shifttype: concept, GenGap Performance

Method	ID MAE(↓)	OOD MAE(↓)
Vanilla	0.0019 ± 0.0004	0.0458 ± 0.0037
Dens	0.0011 ± 0.0001	0.0282 ± 0.0000
Temp	0.0019 ± 0.0004	0.0458 ± 0.0037
MCD	0.9943 ± 0.0008	0.8951 ± 0.0109
G-ΔUQ	0.0011 ± 0.0008**	0.0237 ± 0.0032
Pretr. G-ΔUQ	0.0011 ± 0.0005	0.0188 ± 0.0129

Table 17: GOODMotifLPE-basis, shifttype: covariate, GenGap Performance

Method	ID MAE(↓)	OOD MAE(↓)
Vanilla	0.0000 ± 0.0000	0.5709 ± 0.0128
Dens	0.0000 ± 0.0000	0.5703 ± 0.0000
Temp	0.0000 ± 0.0000	0.5709 ± 0.0128
MCD	0.9992 ± 0.0004	0.4148 ± 0.0057
G-ΔUQ	0.0004 ± 0.0005	0.5729 ± 0.0194
Pretr. G-ΔUQ	0.0004 ± 0.0002	0.5730 ± 0.0041

Table 18: GOODMotifLPE-size, shifttype: concept, GenGap Performance

Method	ID MAE(↓)	OOD MAE(↓)
Vanilla	0.0042 ± 0.0019	0.3244 ± 0.0183
Dens	0.0011 ± 0.0000	0.3148 ± 0.0000
Temp	0.0042 ± 0.0019	0.3244 ± 0.0183
MCD	0.9842 ± 0.0010	0.5629 ± 0.0023
G-ΔUQ	0.0026 ± 0.0013	0.3179 ± 0.0079
Pretr. G-ΔUQ	0.0047 ± 0.0009	0.3076 ± 0.0162

Table 19: GOODMotifLPE-size, shifttype: covariate, GenGap Performance

Method	ID MAE(↓)	OOD MAE(↓)
Vanilla	0.0012 ± 0.0005	0.5376 ± 0.1460
Dens	0.0010 ± 0.0002	0.6273 ± 0.0000
Temp	0.0012 ± 0.0005	0.5376 ± 0.1460
MCD	0.9910 ± 0.0012	0.3586 ± 0.0250
G-ΔUQ	0.0010 ± 0.0012	0.5280 ± 0.1899
Pretr. G-ΔUQ	0.0010 ± 0.0012	0.3564 ± 0.1435

Table 20: GOODSST2-length, shifttype: concept, GenGap Performance

Method	ID MAE(↓)	OOD MAE(↓)
Vanilla	0.0015 ± 0.0004	0.1170 ± 0.0067
Dens	0.0007 ± 0.0001	0.1055 ± 0.0000
Temp	0.0015 ± 0.0004	0.1170 ± 0.0067
MCD	0.9385 ± 0.0028	0.6624 ± 0.0222
G-ΔUQ	0.0021 ± 0.0026	0.1244 ± 0.0168
Pretr. G-ΔUQ	0.0031 ± 0.0017	0.1140 ± 0.0047

Table 21: **GOODSST2-length, shifttype: concept, GenGap Performance**

Method	ID MAE(↓)	OOD MAE(↓)
Vanilla	0.0045 ± 0.0023	0.0566 ± 0.0445
Dens	0.0004 ± 0.0000	0.0479 ± 0.0000
Temp	0.0045 ± 0.0023	0.0566 ± 0.0445
MCD	0.8961 ± 0.0028	0.7954 ± 0.0016
G-ΔUQ	0.0043 ± 0.0024	0.0540 ± 0.0435
Pretr. G-ΔUQ	0.0029 ± 0.0023	0.0302 ± 0.0267